Catalysis Letters 56 (1998) 95–104 

# Influence of intracrystalline diffusion in shape selective catalytic test reactions

Edmund B. Webb III and Gary S. Grest

*Corporate Research Science Laboratories, Exxon Research and Engineering Company, Annandale, NJ 08801, USA*

Received 29 May 1998; accepted 14 October 1998

Molecular dynamics simulations are used to measure the self diffusion constant $D$ of linear decane and $n$-methylnonanes ($n = 2$, 3, 4, and 5) at a catalytically relevant temperature in seven 10 member ring zeolites. Two general behaviors are observed in $D$ as the branch position is moved towards the center of the alkane chain. For three of the zeolites (MEL, MFI, and MTT), $D$ decreases monotonically as expected based on a consideration of the bulkiness of the different isomers. For the other four, alkane diffusion is considered anamolous as $D$ is not a monotonic function of branch position. For $n$-methylnonanes in three zeolites $D$ shows a minimum at either $n = 2$ (FER), 3 (EUO), or 4 (TON). In AEL, $D$ has a local maximum for $n = 3$. Alkane diffusion is anamolous in these zeolites because they have structural features that provide a unique hindrance to molecular motion along the main diffusion channel. The ability of the zeolite to hinder motion depends on the molecular structure of the isoparaffin, resulting in the anamolous behavior observed. The 10 member ring zeolites selected for this study represent the entire group for which known structures exist and values of the modified constraint index have been published. The diffusion data presented indicates that product shape selectivity may play some part in determining the modified constraint index.

**Keywords:** alkane diffusion, zeolites, simulation

## 1. Introduction

Zeolites are a class of microporous materials that possess unique chemical and structural attributes, making them useful in a wide variety of chemical processes. They play a fundamental role in the catalytic upgrading of hydrocarbon fluid streams; for instance, zeolites are used to tailor lubricant basestock properties. While there are many chemical reactions involved in upgrading lubricants, one primary route to achieve this involves controlling the molecular composition through the hydroconversion of paraffins and isoparaffins [1]. The pore or channel structures inherent in zeolites provide part of the functionality that serves in this chemical process. This is believed to be due to the fact that the pore dimensions restrict the motion of bulkier molecules within the structure (i.e., diffusion limitations) or they restrict the types of molecular species that can form in the channels (i.e., configuration limitations). The former restriction can be further divided as to whether it is the reactants or products of a chemical reaction that are hindered by slow diffusion; these two effects are called reactant and product shape selectivity (RSS and PSS). The restriction of chemical configurations is transition-state shape selectivity (TSS) [2]. Due to the import of their channel structures, zeolites are often distinguished in terms of the size of the aluminosilicate ring that is periodically replicated to create the primary pore or channel. Of particular interest to hydroconversion of isoparaffins are zeolites with ten member ring (10 MR) pores. Such pores have dimensions similar to the dimensions of molecular species involved in hydroconversion. As a result, 10 MR zeolites demonstrate unique shape selectivity when used for isomerizing normal and branched alkanes [3–6].

There have been a number of studies to understand the molecular mechanism for hydroconversion in the presence of shape selective zeolites [2–11]. Experimental studies typically analyze the reaction of a well characterized system (feed and catalyst) by measuring the yield of various products as a function of temperature or conversion. By systematically altering parameters of the experimental setup (feed, chemistry of the zeolite, metal dispersion, state point, etc.), these studies aim to infer molecular mechanisms from the observed differences in the products. A review of proposed reaction mechanisms for hydroisomerization and hydrocracking both in the absence and presence of shape selectivity is found in [12]. One way of characterizing unknown zeolites is with test reactions that analyze various product distributions at a specific conversion of a clean alkane feed, such as decane. The resultant data are compared to results for structurally well characterized zeolites [7].

While there are fairly specific descriptions of the chemical mechanisms involved in shape selective hydroconversion, there is still more to learn. For instance, the role of reactant and product diffusion, i.e., RSS and PSS, is a matter of some debate. One test reaction for characterizing 10 MR zeolites is the analysis of methylnonanes created at low conversion of $n$-decane. The modified constraint index ($CI^*$) is defined [7] as the ratio of yields of 2-methylnonane to 5-methylnonane at 5% conversion of $n$-decane. The measure is made at low total conversion to be in the kinetic regime of the hydroconversion process, free from the influence of secondary reactions. Due to the shape selec-

tive nature of 10 MR zeolites, this ratio is typically distinctly higher than what is found in the absence of shape selectivity. Generally, a higher CI* indicates greater spatial constraint or smaller pore dimensions. For a number of 10 MR zeolites, several studies suggest that the selectivity in this test is due to a restriction of bulky transition states for isomerization at the middle of the alkane chain, TSS [4,7]. Support for this interpretation comes from measurements of the diffusion constants at subcatalytic temperature, which found that they were roughly equal for normal decane and the methylnonanes [4]. A study which demonstrated only a small dependence of CI* on particle size (and, therefore, diffusion path) also lends support to this idea [5]. However, there are also experimental studies which have concluded that the contributions of TSS and PSS (i.e., diffusional resistance on bulkier 5-methylnonane molecules) are not trivial to deliniate [12,13]. Clearly, the process of isomerization requires motion of molecules between various sites on the zeolite and, once isomerization is complete, the product molecules must diffuse away from the zeolite to be present in the yield. Depending upon the specific location of isomerization sites, differences in diffusion of the various molecular species could exist and contribute to observed shape selectivity. The order of magnitude for the diffusion constants quoted in [4] indicates that this measurement is probably representative of some macroscopic feature of mass transport rather than intracrystalline diffusion[1]. Furthermore, the measurement was made at a temperature significantly below the catalytic range and the values quoted are quite small which decreases the statistical reliability of a given measure. As such, the validity of these numbers for representing how fast the molecules move through the zeolite structure at catalytically relevant temperatures is questionable. Therefore, more precise knowledge of the transport properties of the molecules is necessary to firmly establish the relevant shape selectivity mechanisms. Besides the CI*, there are other catalytic tests where diffusion is believed to be a primary factor in determining selectivity [12]. Complicating the matter further, there have been recent studies [10,14,15] indicating that, for some zeolite systems, surface or pore-mouth catalysis may play an integral role in the selectivity. Clearly, benefit can be had from more knowledge on the motion of relevant molecules in 10 MR zeolites.

Experimental methods for measuring the diffusion constant $D$ of molecules in frame-work structures exist [16,17] and have been applied to a variety of molecules and structures [9,18–25]. For the same guest molecule and host structure, order of magnitude differences between diffusion constants quoted in the literature are readily found [17,26–28]. The lower values of $D$ are obtained by methods which probe more macroscopic features and not the actual molecular motion itself [28]. In [17], the need to avoid spurious macroscopic contributions for some methods of diffusion measurement is addressed. Despite these complications, certain experimental techniques such as PFG NMR can be used to determine what is considered a microscopic diffusion constant. Unfortunately, studies involving such measurements are often restricted to subcatalytic temperatures, so as to remove the influence of reactions. As a result, these studies are only able to use smaller molecules so that the values of $D$ are within the limit of resolution of the experiment. There are methods for determining relevant diffusion constants from test reactions at catalytic conditions but these depend on presumptions about the influence of diffusion on reactivity that may not be met [9]. As a result, there still exists considerable uncertainty in the experimental ability to accurately describe the dynamics of medium length alkanes in zeolites.

Recently, computer modeling has become an attractive alternate method for studying diffusion in zeolite structures. Specifically, molecular dynamics (MD) simulations provide the ability to study the trajectory of molecules in time. This technique has been applied in a number of studies of diffusion in zeolites [26–35]. The environment and state point of a simulation can be specified precisely and chosen free of the restraints that are imposed on experimental studies. Molecular diffusion constants can be determined directly from the observed mean square displacement (MSD) for a molecule through the Einstein equation for diffusion [36]. The primary limitation to measuring diffusion is the long simulation times needed to obtain reliable statistics. The MSD curve from which $D$ is calculated should demonstrate good linearity in time to allow a reliable measurement of the slope. As discussed in [28], there is an additional requirement in that the MSD of a molecule should be measured over a long enough duration to allow the molecule to completely sample the unit cell of the zeolite. For a diffusion constant of $10^{-10}$ m$^2$/s and a unit cell length of 20 Å, the time necessary to meet the second requirement is 20 ns. In addition, accuracy is improved when multiple time segments are averaged to calculate the MSD. This requires a total simulation duration that is some multiple of the time needed to sample the entire unit cell. MD simulations on the order of tens of nanoseconds for chain molecules of any appreciable length are very computationally intensive. As such, many of the studies employing simulations to measure $D$ have focused on small molecules and used short time trajectories that did not allow the entire unit cell to be sampled. However, advances in computational resources and algorithms have begun to lift this barrier and a recent study [28] was able to observe diffusion for molecules as long as cosane in the zeolite MFI (ZSM-5).

[1] In the paper where the diffusion measurement was quoted [4] the experimental technique was not presented. However, a measurement of hexane diffusion in silicalite at 300 K using PFG NMR [44] gave a value of diffusivity four orders of magnitude larger than the values quoted in [4]. While hexane is smaller than the molecule used in [4] (decane), the PFG NMR measurement was made at a lower temperature. This technique is considered to probe microscopic diffusion, that is the actual molecular motion, rather than macroscopic features of mass transport. Thus, we conclude that the microscopic diffusion of the system probed in [4] was probably much larger and that the value they reported was governed by macroscopic phenomena.

Table 1
Properties of the zeolites studied. The structure type codes, the full type names, the cross section dimensions for the 10 MR channels, and the unit cell parameters are given. The dimensions and parameters are quoted in Å.

| Code | Name | [100] | [010] | [001] | $a$ | $b$ | $c$ |
|---|---|---|---|---|---|---|---|
| AEL | ALPO-11 | $(6.3 \times 3.9)$ | | | 8.4 | 18.5 | 13.5 |
| EUO | EU-1 | $(5.7 \times 4.1)$ | | | 13.7 | 22.3 | 20.2 |
| FER | Ferrierite | | | $(5.4 \times 4.2)$ | 19.2 | 14.1 | 7.5 |
| MEL | ZSM-11 | $(5.4 \times 5.3)$ | $(5.4 \times 5.3)$ | | 20.1 | 20.1 | 13.4 |
| MFI | ZSM-5 | $(5.5 \times 5.1)$ | $(5.6 \times 5.3)$ | | 20.1 | 19.9 | 13.4 |
| MTT | ZSM-23 | | | $(5.2 \times 4.5)$ | 21.5 | 11.1 | 5.0 |
| TON | ZSM-22 | | | $(5.5 \times 4.4)$ | 13.8 | 17.4 | 5.0 |

Herein, we describe results from simulations of decane and its methyl isomers in a collection of 10 MR zeolites. The zeolites that were used in this study represent the entire group of 10 MR systems for which a known crystallographic structure and a modified constraint index ($CI^*$) have been published. The seven zeolites that were used are listed in table 1 by their structure type codes as defined in [37]. Also given there are the full type names, the cross sectional dimensions of channels in each applicable crystallographic direction, and the zeolite unit cell parameter in the corresponding direction. The structure type codes are used to identify the zeolites in this work. For clarification, MTT (ZSM-23) and TON (ZSM-22) have one dimensional, uninterrupted channel structures. As can be seen in table 1, these structures can be distinguished from one another by the dimensions of their channels. AEL ($AlPO_4$-11, isotypic in structure with SAPO-11) has a one dimensional 10 MR channel system whose cross sectional dimensions are the most anisotropic of the zeolites studied. Furthermore, the walls of the pore in the long dimension are periodically interrupted by six member rings on alternate sides of the channel. These rings form the openings to small side pockets which are inaccessible to the molecules studied here. The zeolite EUO (EU-1) also has a one dimensional 10 MR channel system that is interrupted periodically by alternating side pockets. In this structure, the mouths of the side pockets are formed by a 12 MR, so molecules can certainly access these pockets, but diffusion is only possible in the channel direction. Ferrierite (FER) has a one dimensional 10 MR channel system with 8 MR channels running perpendicular to, and intersecting with, the 10 MR channels. For very small molecules, FER can be considered as a two dimensional diffusional structure; however, for the molecules studied here, no transport or even penetration in the 8 MR channels is observed. This is true for the linear alkanes as well as the branched. For this reason, only the 10 MR channels of FER are described in table 1. The remaining two zeolite structures, MFI (ZSM-5) and MEL (ZSM-11), have three dimensional 10 MR channel structures. In MFI, one channel is straight but is intersected by a sinusoidal channel running, on average, perpendicular to the straight channel. In MEL, there are two equivalent and straight channels running perpendicular to one another and also intersecting. In both MEL and MFI, the channel intersections are such that tortuous paths are created which allow diffusion in the direction perpendicular to both the channels. Since motion in the third direction is not along one specific channel, no channel dimensions are provided for that direction. However, the unit cell parameter is given.

To our knowledge, this is the first MD study of linear and branched alkanes of medium length in multiple zeolites. The necessary incorporation of long MD simulation runs for accurately probing such systems further distinguishes this work. Our model and simulation details are briefly described in section 2. In section 3, we discuss the results for diffusion and make comparisons, where possible, with relevant experimental data. Our conclusions are summarized in section 4.

## 2. Model and simulation details

All simulations presented here were done at the infinite dilution limit; that is, molecules inside the zeolite did not interact with one another. This allowed us to focus on how the zeolite pore structure and the molecular shape influence diffusion. It also lowered the computational demands thereby providing the ability to perform longer simulations. This was further facilitated by using a united atom (UA) model to simulate the alkane molecules. In this model, the hydrogen atoms are grouped with the carbon to which they are bonded into a single particle or united atom. Intramolecular interaction between these groups or united atoms is represented by bonded and non-bonded forces. The bonded interactions are represented by three terms. These are constraint forces which keep intramolecular nearest-neighbors at a fixed bond distance, a bending term

$$V_{\mathrm{b}}(\theta) = \frac{k_{\mathrm{b}}}{2}(\theta - \theta_{\mathrm{b}})^2 \tag{1}$$

which maintains the equilibrium angle, $\theta_{\mathrm{b}}$, between successive bonds, and a torsional term

$$V_{\mathrm{t}}(\phi) = \sum_i a_i \cos^i(\phi) \tag{2}$$

characterizing preferred orientations and rotational barriers around all non-terminal bonds. The non-bonded forces are described by Lennard-Jones (LJ) interaction sites located at

Table 2
Lennard-Jones potential parameters.

| Group | $\sigma$ (Å) | $\varepsilon$ (kcal/mol) |
|---|---|---|
| $CH_3$ | 3.930 | 0.227 |
| $CH_2$ | 3.930 | 0.093 |
| CH | 3.850 | 0.064 |
| O | 2.789 | 0.240 |

the position of each carbon atom center of mass. The LJ potential is defined by

$$V_{\mathrm{LJ}}(r) = 4\varepsilon\left[\left(\frac{\sigma}{r}\right)^{12} - \left(\frac{\sigma}{r}\right)^{6}\right]. \tag{3}$$

This non-bonded interaction is between intramolecular sites except for those which are separated by less than four bonds and which, therefore, interact through one or more of the bonded interaction terms. The LJ interaction is truncated at a distance $r_c$ ($r_c = 10$ Å) and the potential is shifted so that $V_{\mathrm{LJ}}(r_c) = 0$. The parameters used for the bonded interactions are those described as Model A in prior bulk simulations of linear and branched alkanes [38]. The parameters for the LJ term are given in table 2; cross terms are calculated from the Lorentz–Berthelot rules [36].

The zeolites simulated were obtained directly from the zeolite structure database contained in the *Insight II* software package [39]. As such, the structures used represent idealized stoichiometry and crystal structure. For a zeolite with an $n$ dimensional channel system, the unit cell was replicated in the appropriate $n$ crystallographic directions. A minimum amount of zeolite material was used that would still permit appropriate application of $n$ dimensional periodicity. Since alkane molecules were unable to diffuse in non-periodic directions it was only necessary to include zeolite material in those directions sufficient to guarantee saturation of the alkane/zeolite interaction. The zeolite lattice was held rigid throughout the simulations. Since the focus was on the changes in diffusion between different molecules and structures, rather than a high degree of accuracy for a given number, this was deemed acceptable. The LJ potential was used for interactions between the isoparaffins and the zeolite. Furthermore, it was assumed that the large oxygen anions would strongly dictate the shape of the force field experienced by the alkanes, so framework Si (and, in the case of AEL, Al and P) were negelected from the LJ calculation. The LJ parameter used for oxygen interactions, therefore, represents an effective parameter for calculating the overall zeolite force field. These same approximations for representing the zeolite and the alkane/zeolite interaction have been used in the past [26,28,40,41]. Different from these prior works, we distinguish between $CH_n$ groups for the alkane/zeolite interactions. This change was made since we included branched alkanes in the study. The LJ parameters for zeolite oxygens were calculated from the values used in [27] by normalizing with respect to normal decane in our model. While the model was not able to probe chemical reactions it permitted a clear investigation of how the pore structure and alkane molecular shape influence diffusion.

All simulations presented here were done at $T = 600$ K, which is somewhat in the middle of the catalytic operating temperature range. Since the zeolite was static and the molecules did not interact with one another, it was necessary to thermostat the alkanes using a stochastic force method. The time constant used for the stochastic thermostat was $\tau = 1$ ps. The equations of motion were integrated using the velocity Verlet algorithm [36] and bond lengths were kept constant using the RATTLE algorithm [36].

Simulations were begun by placing 64 all *trans* versions of a molecule in the main diffusion channel with the molecular axis collinear with the channel axis. Each of the 64 molecules was given a random rotation about the channel axis and shifted along the channel a random amount. Initial high energy configurations were relaxed by a 2 ps run using a 1 fs time step ($\delta t = 1$ fs) at 900 K; all subsequent simulations used either $\delta t = 4$ or 5 fs. Systems were then run at $T = 900$ K for 1 ns to randomize the molecular positions further. Another 1 ns run at 600 K was performed to reach the appropriate temperature. Since simulations were done in the dilute limit, equilibrium was considered attained once the 64 molecules were evenly distributed throughout the unit cell. In certain systems, it was deemed necessary to allow additional time for equilibration. Predominantly, this was the case for slow moving molecules in complex channel structures. After equilibration, runs in the range of 6–40 ns were done to measure diffusion. Due to the constraint imposed by the zeolite channels and the simulation temperature for gathering diffusion, there was concern that a 5 fs time step might be too large, increasing the systematic error in the diffusion measurement. Select simulations were performed at different time steps to address this. Comparisons between simulations at $\delta t = 4$ and 5 fs showed essentially no difference at 600 K. With $\delta t = 2.5$ fs, a small shift in diffusion was observed (less than 20%) at 600 K. For a given zeolite, this shift was consistent for different molecules so relative diffusion constants stayed roughly the same. Since our primary goal here was to compare relative diffusion constants between zeolites, we used results from simulations at $\delta t = 4$ or 5 fs.

The diffusion constant was obtained, as described in section 1, from the Einstein equation for diffusion:

$$D = \frac{\langle (r(t) - r(0))^2 \rangle}{6t}. \tag{4}$$

The angle brackets are used to denote an ensemble average over the 64 (isolated) molecules and all available initial times (i.e., a block averaging technique [36] was used). Due to the anisotropic nature of diffusion in zeolites, it was useful to consider diagonal terms of the diffusion tensor. For the $x$ direction,

$$D_x = \frac{\langle (x(t) - x(0))^2 \rangle}{2t}, \tag{5}$$

with similar expressions for the $y$ and $z$ directions.

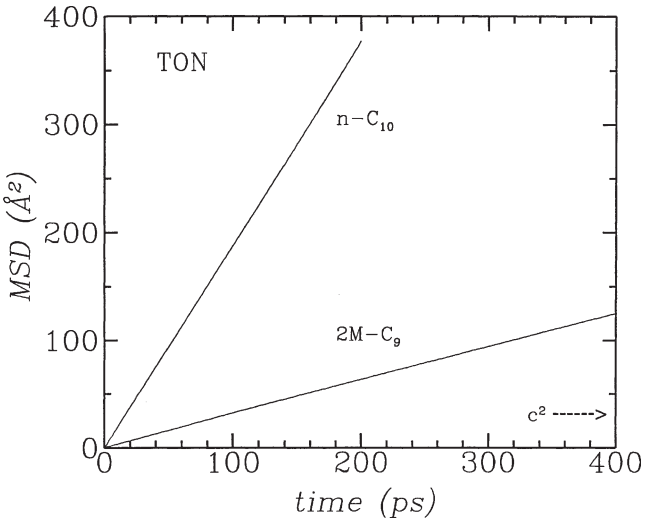


Figure 1. Mean square displacement (MSD) as a function of time for $n$-decane and 2-methylnonane in TON. The square of the value of the unit cell parameter in the diffusion channel direction is indicated on the $y$-axis.

## 3. Results and discussion

Figure 1 shows the mean square displacement (MSD) in the channel direction for $n$-decane and 2-methylnonane in TON. As can be seen from this figure, both conditions outlined in section 1 are met for statistical reliability of the MSD curve and $D$ thereby obtained. That is, there is good linearity and the molecules were able, on average, to sample at least an entire unit cell of TON in the time over which the MSD was measured. Figure 2(a) shows the MSD curve for $n$-decane in MTT; figure 2(b) shows the MSD curve for 2-methylnonane in MTT (note the change in $y$-axis range between figure 2 (a) and (b)). Figure 2(b) shows that the branched alkane is not able, on average, to sample an entire unit cell during the time over which the MSD was measured. There were other cases of slow moving molecules where this was also the case. While this indicates a larger error for the lowest values of diffusion that we have measured, the numbers presented are still fairly reliable because we averaged over 64 molecules placed at different initial positions along the unit cell and total run times that were much longer than the duration over which the MSD curves were measured. In prior work [38], the error in values of $D$ obtained with our model was roughly 5%. For the temperature and time step used herein, we anticipate that error in diffusion measurements is less than 10% for most molecules and between 10 and 25% for the lowest values of $D$ measured.

For the purpose of comparison with [28], a simulation of $n$-decane in MFI at $T = 400$ K was performed. The diffusion constant thereby obtained agreed with the value quoted in [28] to within 10%. The values of $D$ obtained in their work were greater than values of $D$ obtained with experimental techniques; however, their work was found to give order of magnitude agreement with experimental methods that probe "microscopic" diffusion such as PFG

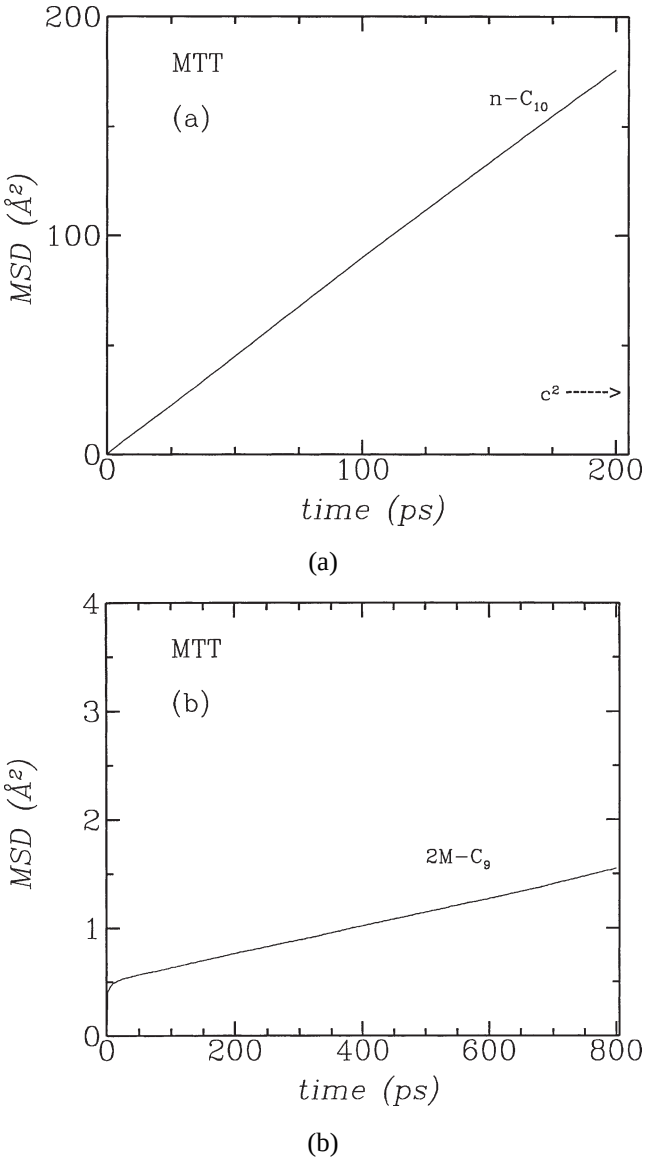


Figure 2. (a) MSD for $n$-decane in the zeolite MTT. (b) MSD for 2-methylnonane in MTT (the $y$-axis ranges for (a) and (b) are different).

NMR. As this implies a comparable level of agreement for our model, we take this as support that our model parameters are reliable. Most importantly, we are interested in how diffusion changes going from one molecule to another in a given structure and, if this change is large, order of magnitude agreement allows such a comparison to be made with good reliability. As also discussed in [28], we expect that the values of $D$ obtained herein represent upper limits. The reasons for this are the use of a static and defect-free zeolite lattice, the condition of infinite dilution, and the use of an united atom model for the alkanes.

Table 3 contains the diffusion constant calculated for all the molecules in each of the seven zeolite structures. For MFI, only the data for the fastest (straight) channel is presented; for MEL, the values of $D$ quoted represent both of the main channels as they are identical in structure. Diffusion constants for the two other directions in MFI and the

Table 3
Diffusion constant $D$ for each molecule in the seven zeolites studied. The $D$ quoted are $\times 10^{10}$ m$^2$/s.

| Zeolite | $n$-$C_{10}$ | 2M-$C_9$ | 3M-$C_9$ | 4M-$C_9$ | 5M-$C_9$ |
|---|---|---|---|---|---|
| AEL | 151.7 | 8.2 | 34.5 | 18.5 | 6.3 |
| EUO | 8.7 | 0.32 | 0.22 | 0.9 | 1.1 |
| FER | 173.6 | 4.8 | 6.6 | 13.3 | 17.4 |
| MEL | 27.7 | 0.20 | 0.14 | 0.07 | 0.05 |
| MFI | 55.9 | 1.2 | 0.22 | 0.14 | 0.09 |
| MTT | 42.0 | 0.044 | 0.04 | 0.02 | 0.019 |
| TON | 95.8 | 14.8 | 0.84 | 0.18 | 0.59 |

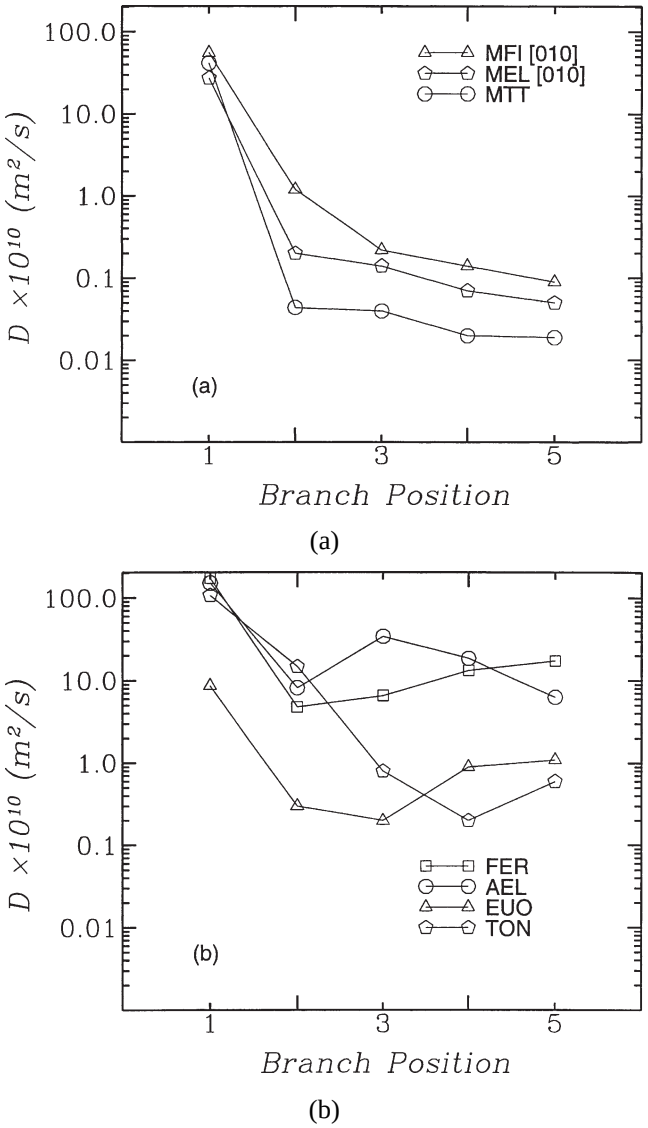


Figure 3. Diffusion constant as a function of branch position: (a) the three zeolites for which $D$ monotonically decreases with higher branch position, (b) the remaining structures for which $D$ is not a monotonic function of branch position.

third direction in MEL were calculated and are given elsewhere [42]. In figure 3 (a) and (b), the diffusion constants are plotted as a function of branch position with branch position 1 representing the linear molecule. As seen in figure 3(a), order of magnitude changes are observed for a shift of one position for the branch, in certain instances. Clearly, diffusion constants shown in the table and figure are different for the different isomers of $C_{10}$. The behavior is not surprising since, as a branch is moved towards the center of the chain, the molecule's motion is more hindered by interactions with the channel wall. For all seven zeolites the diffusion for $n$-decane is larger than for the $n$-methylnonanes. This demonstrates the increased bulkiness of $n$-methylnonane molecules with three $CH_3$ groups compared to $n$-decane with two $CH_3$ groups. If motion between active sites inside a zeolite is required for isomerization to be completed and a product molecule to be realized in the yield, data presented in figure 3 indicates that product shape selectivity could influence the observed yields when isomerizing linear alkanes.

Note that $D$ is not always a monotonic function of branch position. In three of the structures, $D$ reaches a minimum at either the 2 (FER), 3 (EUO), or 4 (TON) branch position. In AEL, $D$ reaches a local maximum at the 3 branch position. For these structures, the increased bulkiness of the alkane molecules as the branch is moved towards the center of the chain does not successively slow diffusion as occurs for MEL, MFI, and MTT. This unexpected behavior of $D$ can be explained by observation of the dynamics of individual molecules inside the zeolites. Pictures of the system can be used to illustrate aspects of a molecule's motion that determine its overall diffusion. Results are shown in figure 4 (a)–(i) for $n$-decane, 2-methylnonane, and 5-methylnonane in AEL, EUO, and FER (the graphics package VMD [43] was used to make these pictures). In each of the nine snapshots, only a section of the zeolite framework is displayed to emphasize the pertinent structural features of the channel.

As can be seen from the channel dimension data in table 1, the channels in AEL are highly asymmetric. As a result, alkane molecules are rather constrained in the direction corresponding with the short dimension but not in the long dimension. In figure 4(a) it can be seen that the walls of the AEL channels are periodically interrupted by small rings on alternating sides of the channel in the long dimension. For $n$-decane, the zeolite's structure produces a minimum resistance to molecular motion and $D$ for $n$-decane is the second highest in AEL for the zeolites studied. The presence of a branch means another $CH_3$ group must be accomodated by the zeolite. In AEL, this is best done at the 6 MR openings to the small side pockets in the channel wall. The centers of these rings are the most energetically favorable spots for $CH_3$ groups to reside as they optimize interactions with the channel wall. This means that molecular motion of the monobranched nonanes in AEL is dominated by a competition amongst $CH_3$ groups to situate themselves at the energetically favorable positions along the channel. This is illustrated for 2-methylnonane in figure 4(b) as the molecule tends to position the end with the two $CH_3$ groups near the center of a 6 MR. Diffusion down the channel is accomplished by jumps between successive pocket mouths. When the branch is at the 3 position, the frequency of these jumps

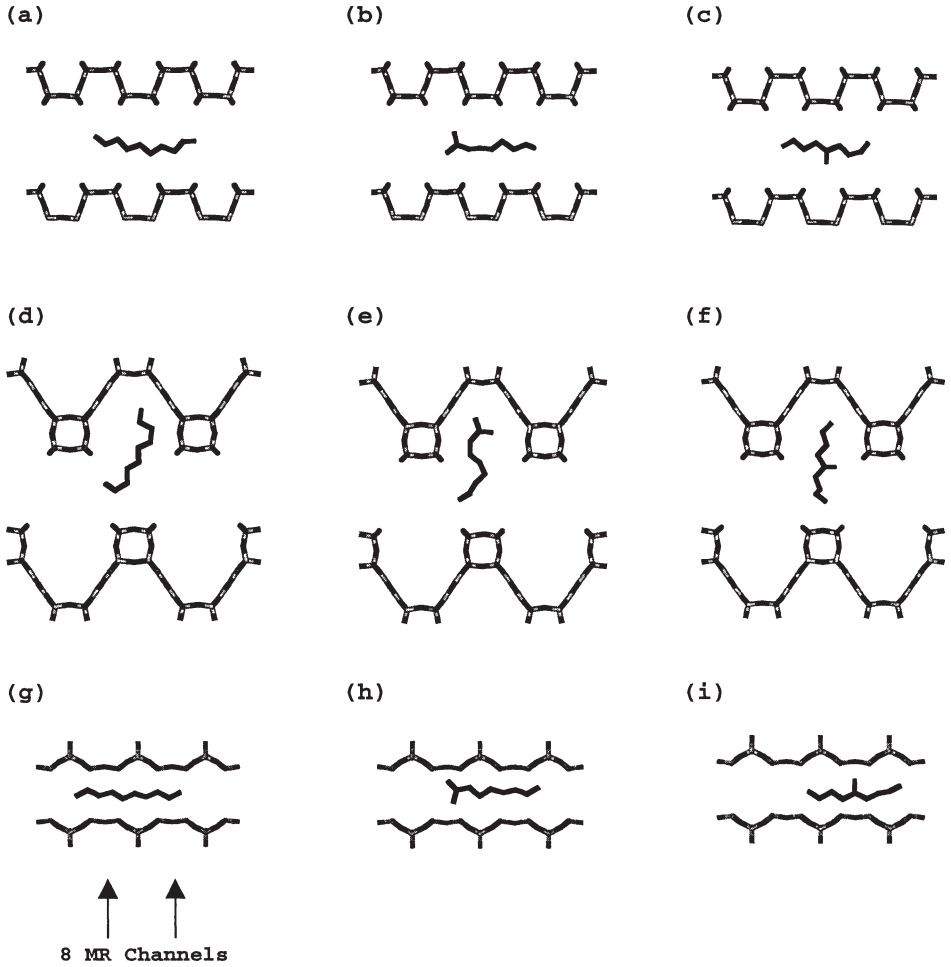


Figure 4. Snapshots of $n$-decane, 2-methylnonane, and 5-methylnonane in the zeolites AEL (a)–(c), EUO (d)–(f), and FER (g)–(i). Note that the long dimension of the diffusion channel in AEL is shown.

is greater resulting in higher diffusion. This is a direct result of the relationship between the $CH_3$ spacing along the molecule and the side pocket spacing along the channel wall. For 3-methylnonane, this relationship results in the lowest energetic barrier to diffusional jumps for all the methylnonanes in AEL. For 4-methylnonane, the relationship is not as good, so diffusion is lower than for 3-methylnonane, though still higher than either 2 or 5-methylnonane. Figure 4(c) demonstrates that the AEL structure is able to accomodate all $CH_3$ groups at successive favorable positions along the channel for 5-methylnonane. The energetic barrier to jumping along the channel is greatest and $D$ for 5-methylnonane is the lowest.

A similar situation was observed for $n$-alkanes in MFI by Runnebaum and Maginn [28]. In their work, diffusion generally decreased with chain length except for certain resonant chain lengths where a local maximum in $D$ was observed. They explained the behavior as resulting from a relation between the molecule length and spacing between intersections along the zeolite channel. For AEL, we explain the resonant branch position as resulting from a relation between the separation distance of $CH_3$ groups and the spacing between successive side pocket openings along the zeolite channel. In AEL and, as will be discussed, in EUO, FER, and TON the relation between the methylnonane structure and the zeolite structure is more influential than the increased bulkiness as a branch is moved towards the center of the chain. This is demonstrated by the anamolous variation of $D$ with branch position.

For EUO, the side pockets perpendicular to the main channel represent molecular traps because they do not allow diffusion in the perpendicular direction and they are accessed through a relatively large pore (i.e., a 12 MR opening). The size of the pockets is such that interactions between an alkane molecule and the zeolite are optimized when the alkane inserts one of its $CH_3$ end groups into the pocket. Thus, there is a high probability that linear molecules will sample the space inside these pockets for some period of time, before hopping down the main channel to another side pocket, or trap. This behavior is illustrated in figure 4(d) where $n$-decane is seen to reside in a side pocket. The result is that jumps down the diffusion channel are infrequent and $D$ for $n$-decane is lower in EUO than the other zeolites studied. When a branch is put on a linear chain at the 2 position in EUO, the molecule becomes bulkier but the zeolite structure readily accomodates this as

both $CH_3$ groups at the methylated end are able to reside in a side pocket. This is shown in figure 4(e). These hindrance effects of a bulkier molecule and efficient trapping by the side pockets combine so that the $D$ is lowered dramatically. The 3-methylnonane molecule is even bulkier and the diffusion constant lowers further. However, the change in the value of $D$ between the 1 and 2 positions is greater than the change between the 2 and 3 positions. This is partly because the side pockets cannot trap both the $CH_3$ groups at the methylated end as efficiently as they could for 2-methylnonane. As the branch is moved closer to the center of the chain, the fit of two $CH_3$ groups in a side pocket becomes worse and diffusion is higher for 4-methylnonane than either 2- or 3-methylnonane. When 5-methylnonane inserts an end $CH_3$ group into a side pocket, the branch group is forced to reside at the entrance to the pocket, as can be seen in figure 4(f). This situation represents the least efficient trapping for the methylnonanes so, despite the bulkier nature of 5-methylnonane, its diffusion constant is higher than the other methylnonanes. In EUO, the dominant relation between the zeolite structure and the molecule structure is represented by the ability of the zeolite's side pockets to trap molecular segments. As the branch position is moved towards the center of the isoparaffin chain, the ability to fit two $CH_3$ groups in the side pockets decreases so hindrance to molecular diffusion is lower.

The behavior in FER can be explained in a similar fashion. For AEL and EUO, side pockets are along the main channel on alternate sides as one moves down the channel. In FER, 8 MR channels intersect the main channel and so a void space is present on both sides of the main channel at an intersection point, as is shown in figure 4(g). These voids do not hinder the motion of the linear alkane and $D$ in FER for $n$-decane is the highest of the zeolite structures studied. When a branch is added at the 2 position, the molecule's added bulkiness is readily accomodated by the zeolite structure. This is because the two $CH_3$ groups at one end of the chain occupy void spaces which are the entrances to the 8 MR channels on either side of the main channel. An illustration of this is given in figure 4(h). Thus, the methylated end of the chain positions itself at an intersection point and is fairly well locked there. Diffusion down the main channel for 2-methylnonane is accomplished by jumps from one intersection to another but these jumps are relatively infrequent since the fit of the $CH_3$ groups to the void spaces is good. When the branch is moved to the 3 position, the methyl carbons are further apart. This disrupts the commensurability between the molecular structure and the voids present at intersections in the main channel. The molecule is less efficiently locked to an intersection position, so hops to adjacent intersections occur more frequently. As a result, 3-methylnonane diffuses faster than 2-methylnonane. When the branch position is in the middle of the chain, it is not possible for two of the $CH_3$ groups to occupy void spaces at intersections. As demonstrated in figure 4(i), the branched group preferentially resides at intersections. The relationship between the molecule's and the zeolite's structure is such that hops occur even more frequently and diffusion amongst the branched isomers is fastest for 5-methylnonane in FER.

Table 4
The modified constraint index, CI*, and the ratio of the diffusion constant for 2-methylnonane to 5-methylnonane for the seven zeolites studied.

| Zeolite | CI* | $D_{2MC_9}/D_{5MC_9}$ |
|---|---|---|
| TON | (12.0–15.0)[a] | 25.1 |
| MFI | (3.0–12.0)[b] | 13.3 |
| MEL | (2.8–11.0)[b] | 4.2 |
| AEL | (3.3–3.6)[c,d] | 1.3 |
| EUO | (1.4–2.2)[d] | 0.3 |
| MTT | (10.8–11.1)[c,e] | 2.3 |
| FER | (8.2–10.5)[e] | 0.3 |

[a] From [10].
[b] From [8].
[c] From [12].
[d] From [5].
[e] From [6].

The cause of the anomalous diffusion behavior in TON is the most subtle observed. The channel structure of TON is absent of any side pockets or channel intersections like those in AEL, EUO, and FER. The increase in diffusion for 5-methylnonane compared to 4-methylnonane appears to be related to the unit cell dimension in the channel direction. This value, 5.04 Å, is nearly equal to the average length of molecule segment on either side of the branch when the branch is at the 5 position. While subtle, there is an energetically favorable position for $CH_3$ groups to reside along the TON channel. When the spacing between successive $CH_3$ groups is equal to the unit cell dimension, it is also equal to the spacing between these positions. At this condition, jumps to successive sites along the channel are more likely and diffusion is slightly enhanced.

For each of the seven zeolites, table 4 lists the modified constraint index (CI*) and compares this to the ratio of $D$ for 2-methylnonane to $D$ for 5-methylnonane. Recall that CI* is defined [7] as the ratio of yields of 2-methylnonane to 5-methylnonane at 5% conversion of $n$-decane. For each of the zeolites, a range is reported for CI* demonstrating the variability of these values as reported in the literature. At least for MEL and MFI, the higher values can be ascribed to smaller Si : Al ratios [5]. More systematic studies such as the one in [5] are necessary to clarify the range and dependence of CI* on various catalyst parameters in other zeolites. If product shape selectivity plays an integral part in determining the CI*, one would expect the ratio of diffusion constants to relate to the CI*. For five of the zeolites tested, table 4 shows that ordering of the zeolites by CI* is practically the same if they are ordered according to the ratios of the diffusion constants. In fact, the magnitudes of the reported values of CI* are similar to the magnitudes of the ratios. Considering the variability of the CI* as reported in the literature and the absence of compositional variation and loading effects in our model, the level of correlation observed is significant. At least for these five structures,

it appears that product shape selectivity may play a part in determining the value of CI*. At the very least, molecular diffusion should be considered when interpreting CI*.

MTT was one of the structures which did not order properly by its ratio of diffusion constants. For this structure, however, diffusion of the branched alkanes was the lowest observed. For 2-methylnonane in MTT, the MSD data presented in figure 2(a) demonstrates that it takes roughly 40 ns for the molecule to move a distance equal to the unit cell parameter. It is thus expected that diffusion constants quoted for branched alkanes in MTT are subject to the largest error. It is possible that, for this zeolite, we are obtaining only order of magnitude accuracy. This may partly explain the lack of correlation between the CI* and the ratio of diffusion constants for this structure. The other structure which did not order properly by its diffusion constants ratio, FER, was one of the structures which demonstrated anamolous diffusion behavior for the isoparaffins. In this instance, diffusion of 2-methylnonane was slower than 5-methylnonane, so the ratio of the diffusion constants was less than one. In general, 10 MR zeolites have a CI* greater than two due to shape selectivity imposed by the narrow channels. From the data presented, product shape selectivity does not appear to be influential in determining CI* for FER. Despite the proper ordering for EUO, a similar concern can be raised since its diffusion constant ratio was also less than one. However, for EUO, data has been presented recently [6] that indicates a significant part of the catalytic activity may be occurring on the surface of zeolite crystals. This may be part of the reason for the failure of the diffusion constants ratio to correlate more directly with the CI*. It is also possible that the dependence of the ratio of diffusion constants upon molecular loading is a function of the zeolite. Unfortunately, data presented are insufficient to explain these observations unequivically.

## 4. Conclusion

Diffusion of the isomers of decane inside seven 10 MR zeolites has been reported. Contrary to previous work [4], differences in the diffusion constants for the different molecules are present in all the zeolites studied here. While transition-state shape selectivity has been quoted as the primary factor in determining methylnonane yields on isomerizing $n$-decane, data presented here clearly demonstrates that product shape selectivity cannot be fully discounted. For five of the seven zeolites tested, ordering them according to their modified constraint index (CI*) is the same as ordering them according to the ratio of the diffusion constants for 2-methylnonane to 5-methylnonane. A complete explanation for the failure of the two other zeolite's diffusion constant ratios to properly correlate with their values of CI* cannot be provided.

## Acknowledgement

We thank Maurizio Mondello for work on developing the MD code used in this study. We also thank Jack Johnson, Dan Leta, Gary McVicker, Liam Murphy, Stu Soled, and David Vaughan for many helpful discussions.

## References

[1] S.J. Miller, in: *Extended Abstracts 206th ACS Meeting, Division of Petroleum Chemistry*, American Chemical Society (VCH, New York, 1993) p. 788.
[2] W.O. Haag, R.M. Lago and P.B. Weisz, Faraday Disc. Chem. Soc. 72 (1982) 317.
[3] H.L. Coonradt and W.E. Garwood, Ind. Eng. Chem. Proces Eng. Data 3 (1964) 38.
[4] P.A. Jacobs, J.A. Martens, J. Weitkamp and H.K. Beyer, Faraday Discuss. Chem. Soc. 72 (1982) 353.
[5] J.A. Martens and P.A. Jacobs, Zeolites 6 (1986) 334.
[6] W. Souverijns, L. Rombouts, J.A. Martens and P.A. Jacobs, Micropor. Mater. 4 (1995) 123.
[7] J.A. Martens, M. Tielen, P.A. Jacobs and J. Weitkamp, Zeolites 4 (1984) 98.
[8] P.A. Jacobs and J.A. Martens, Pure and Appl. Chem. 58 (1986) 1329.
[9] P. Voogd and H. van Bekkum, Appl. Catal. 59 (1990) 311.
[10] J.A. Martens et al., Appl. Catal. 76 (1991) 95.
[11] D.S. Santilli, T.V. Harris and S.I. Zones, Micropor. Mater. 1 (1993) 329.
[12] J. Weitkamp and S. Ernst, Catal. Today 19 (1994) 107.
[13] S. Ernst, J. Weitkamp, J.A. Martens and P.A. Jacobs, Appl. Catal. 48 (1989) 137.
[14] J.A. Martens et al., Angew. Chem. Int. Ed. Engl. 34 (1995) 2528.
[15] W. Souverijns et al., in: *Studies in Surface Science and Catalysis*, Vol. 105, eds. H. Chon, S.K. Ihm and Y.S. Uh (Elsevier, New York, 1997) pp. 1285–1292.
[16] J. Karger and D. Ruthven, *Molecular Transport and Reaction in Zeolites Design and Application of Shape Selective Catalysts* (Wiley, New York, 1990).
[17] N.Y. Chen, J. Thomas, F. Degnan and C.M. Smith, *Molecular Transport and Reaction in Zeolites Design and Application of Shape Selective Catalysts* (VCH, New York, 1993).
[18] Y. Yasuda and A. Yamamoto, J. Catal. 93 (1985) 176.
[19] M. Goddard and D.M. Ruthven, Zeolites 6 (1986) 445.
[20] J. Kaerger and H. Pfeifer, Zeolites 7 (1987) 90.
[21] D.T. Hayhurst and A. Paravar, Zeolites 8 (1988) 27.
[22] K. Beschmann, S. Fuchs and L. Riekert, Zeolites 10 (1990) 798.
[23] W. Niessen and H.G. Karge, Stud. Surf. Sci. Catal. 60 (1991) 213.
[24] M.A. Jama, M.P.F. Delmas and D.M. Ruthven, Zeolites 18 (1997) 200.
[25] S.C. Reyes et al., J. Phys. Chem. B 101 (1997) 614.
[26] R.L. June, A.T. Bell and D.N. Theodorou, J. Phys. Chem. 96 (1992) 1051.
[27] E.J. Maginn, A.T. Bell and D.N. Theodorou, J. Phys. Chem. 100 (1996) 7155.
[28] R.C. Runnebaum and E.J. Maginn, J. Phys. Chem. B 101 (1997) 6394.
[29] C.R.A. Catlow et al., J. Chem. Soc. Faraday Trans. 87 (1991) 1947.
[30] S.J. Goodbody et al., J. Chem. Soc. Faraday Trans. 87 (1991) 1951.
[31] M. Kawano, B. Vessal and C.R.A. Catlow, J. Chem. Soc. Chem. Commun. 12 (1992) 879.
[32] J.B. Nicholas et al., J. Phys. Chem. 97 (1993) 4149.
[33] D. Dumont and D. Bougeard, Zeolites 15 (1995) 650.
[34] G. Schrimpf, B. Tavitian and D. Espinat, Revue de L'Institut Francais du Petrole 50 (1996) 105.
[35] D. Keffer, A.V. McCormick and A.T. Davis, Molec. Phys. 87 (1996) 367.

[36] M.P. Allen and D.J. Tildesley, *Computer Simulation of Liquids* (Clarendon, Oxford, 1987).
[37] W.M. Meier and D.H. Olson, *Atlas of Zeolite Structure Types* (Butterworth–Heinemann, London, 1992).
[38] M. Mondello and G.S. Grest, J. Chem. Phys. 103 (1995) 7156; 106 (1997) 9327.
[39] Molecular Simulations Inc., San Diego, CA.
[40] A.V. Kiselev, A.A. Lopatkin and A.A. Shulga, Zeolites 5 (1985) 261.
[41] B. Smit and J.I. Siepmann, J. Phys. Chem. 98 (1994) 8442.
[42] E.B. Webb and G.S. Grest, in preparation.
[43] W. Humphrey, A. Dalke and K. Schulten, J. Molec. Graphics 14 (1996) 33.
[44] W. Heink et al., J. Chem. Soc. Faraday Trans. 88 (1992) 3505.